Journal of Motor Behavior, 2005, Vol. 37, No. 1, 35–51

The Excitator as a Minimal Model for the Coordination Dynamics of Discrete and Rhythmic Movement Generation

Viktor K. Jirsa
J. A. Scott Kelso
Center for Complex Systems and Brain Sciences
Florida Atlantic University, Boca Raton

ABSTRACT. The authors identify a class of excitable two-dimensional model systems, the *excitators*, that provide an entry point to the understanding of the mechanisms of discrete and rhythmic movement generation and a variety of related phenomena, such as false starts and the geometry of phase space trajectories. The starting point of their analysis is the topological properties of the phase flow. In particular, the phenomenon of false starts provides a characteristic structural condition for the phase flow, the separatrix, which partitions the phase space. Threshold phenomena, which are characteristic of excitable systems, as well as stable and unstable fixed points and periodic orbits, are discussed. Stable manifolds in the proximity of fixed points, resulting in an overshoot and a slow return phase after movement execution, are predicted in the analysis. To investigate coordination phenomena, the authors discuss the effects of two types of couplings, the sigmoidal coupling and a truncated version thereof, known as the Haken-Kelso-Bunz (HKB) coupling. They show analytically and numerically that the sigmoidal coupling leads to convergence phenomena in phase space, whereas the HKB coupling displays convergent as well as divergent behaviors. The authors suggest a specific representation of the excitator that allows the quantification of the predictions.

Key words: convergence, coupling, divergence, false start

One may causally describe how limb movements are controlled under the conditions of a changing environment by using a variety of approaches, each emphasizing different facets of the problem. In biomechanically based models, one approaches the dynamics of limb motion by using the idea that muscles can behave like complex springs (Balasubramaniam & Feldman, 2004; Feldman, 1980a, 1980b). The flexor and extensor muscles are idealized as springs that exert forces on masses, primarily the bone of the limb. If those forces are in equilibrium, then the limb is at rest. The motor system accomplishes movement control by changing the parameters of the mass–spring system such that the equilibrium point shifts and the now destabilized system seeks to move toward the new equilibrium point. That, and closely related principles, are known in the literature as *equilibrium controls*, in particular the α models (Polit & Bizzi, 1978, 1979) and the λ models (Balasubramaniam & Feldman, 2004; Feldman, 1980a, 1980b). It is fairly well accepted that the equilibrium models provide a good account of how a joint or limb achieves its terminal position (see Kelso, 1977; Kelso, Southard, & Goodman, 1979; Schmidt & McGown, 1980) and are well suited for describing discrete movement tasks. To describe rhythmic tasks involving the periodic joint motion between two positions, a model has to provide for periodic equilibrium-point control, which hence would result in an externally driven system. In another type of approach, often referred to as the *dynamical systems approach*, the importance of structures and symmetries within the dynamics of the observable is emphasized, and the identification of the material elements (e.g., muscles, tendons) underlying the observed dynamics is of less concern. Examples are the Haken-Kelso-Bunz (HKB) model (Haken, Kelso, & Bunz, 1985), which describes bimanual rhythmic movement coordination; the model of Schöner (1990), which extends the HKB model to discrete movements; and the model of Sternad, Dean, and Schaal (2000), which is also capable of describing discrete and rhythmic movement generation. The HKB model is a system of two nonlinearly coupled limit cycle oscillators that are realized by Van der Pol–Rayleigh oscillators. The relative phase between the two limit cycles exhibits stable in-phase and antiphase coordination, of which the latter is destabilized through a pitchfork bifurcation as the movement frequency is increased. Schöner suggested a modification of the intrinsic dynamics of that set

Correspondence address: Viktor K. Jirsa, Center for Complex Systems and Brain Sciences, Florida Atlantic University, Boca Raton, FL 33431, USA. E-mail address: jirsa@ccs.fau.edu

of oscillators but did not alter the coupling. The modified dynamics is based on a model by Gonzalez and Piro (1987) that displays two stable fixed points for one parameter setting and the existence of a stable periodic orbit for another parameter setting. Here the motor system achieves movement control by changing the model parameters for specific time windows, thus stabilizing or destabilizing the stationary solutions appropriately.

The model of Sternad et al. (2000) consists of two units—one limit cycle (rhythmic) and one point attractor (discrete)—that are coupled by mutually inhibitory connections. Because of the coupling, step changes to the discrete unit shift the center of oscillation in a phase-dependent manner, which captures the observed pattern in experimental data. Evidence from neuroscience studies—in particular, recent functional magnetic resonance imaging studies—shows that different cortical subsystems contribute to the generation of synchronized and syncopated movement (Mayville, Jantzen, Fuchs, Steinberg, & Kelso, 2002) in addition to a common cortical control. In particular, syncopation has been interpreted as "executed individually on each perception-action cycle" (Mayville et al., p. 214), implying the character of a discrete movement. Several attempts have been made to attribute neuroscientific meaning to the model equations of the dynamical systems approach. Grossberg, Pribe, and Cohen (1997; Pribe, Grossberg, & Cohen, 1997), as well as Nagashino and Kelso (1992), used neural oscillator equations to reproduce stabilization and destabilization phenomena of the relative phase found in bimanual coordination. Similarly, to understand lag-one correlation effects as obtained from the continuation paradigm used by Wing and Kristofferson (1973), Beek, Peper, and Daffertshofer (2002) postulated an interplay between neural fields and the behavioral effectors. Jirsa and Haken (1996, 1997) have developed such neural fields in the context of magnetoencephalographic (MEG) studies of sensorimotor coordination and control (Fuchs, Kelso, & Haken, 1992; Jirsa, Friedrich, Haken, & Kelso, 1994; Kelso et al., 1992). More general treatments of neural fields have been discussed extensively in the literature (Amari, 1977; Haken, 1996, 2002; Jirsa, 2004; Jirsa & Haken, 1996; Jirsa & Kelso, 2000; Nunez, 1974, 1995; Robinson, Rennie, & Wright, 1997; Wilson & Cowan, 1972, 1973; Wright & Liley, 1996). Following the introduction of the bimanual rhythmic coordination paradigm (Kelso, 1981), the underlying spatiotemporal brain activity has been mapped onto movement and coordination variables in several brain-imaging studies (Fuchs, Jirsa, & Kelso, 2000; Fuchs et al., 1992; Fuchs et al., 2000; Jirsa, 2004; Jirsa, Friedrich, & Haken, 1995; Kelso et al., 1992; Kelso et al., 1998; Meyer-Lindenberg, Ziemann, Hajak, Cohen, & Berman, 2002). In particular, the behavioral HKB equations were successfully derived from neural field equations (Daffertshofer, Peper, & Beek, 2004; Jirsa, Fuchs, & Kelso, 1998), allowing for an interpretation of the phenomenological coupling terms.

In the present article, we identify a minimal model of discrete and rhythmic movement generation that encapsulates all the dynamic features just discussed. Phenomena such as false starts and trajectory shapes may be understood on the basis of our proposed model. We discuss the dynamics analytically and provide theoretical proof that the HKB coupling, and generalized forms thereof, always results in a convergence or a divergence of the movement patterns, depending only on the initial limb positions. The proof is valid irrespective of the specific type of coordination; thus, it is true for both discrete and rhythmic movement patterns. In our approach, we emphasize symmetry and topological arguments. However, there are several implications that hint at connections to an underlying neural basis, grounded primarily on the similarity between the model developed here and a variety of equations describing neuronal dynamics, such as the FitzHugh–Nagumo system (FitzHugh, 1961). We discuss the intrinsic dynamics of the proposed model in the next section and the coupled dynamics of two such model systems in the following section. In the last section, we summarize and conclude this article.

Intrinsic Dynamics of the Excitator

Trajectory Formation in Phase Space: Theory

A *false start* is the act of beginning a behavior at an inappropriate moment in time. The behavior may be fully or only partially executed. In language production, a false start is the act of beginning an utterance and typically aborting it before completion. False start errors, which occur most often when a conversation becomes intense, are used in the quantitative study of speech impairment (Croot, Hodges, Xuereb, & Patterson, 2000). In sports and movement sciences, a false start, for example, in sprinting (Collet, 1999), is the initiation of a movement before the signal of the starter.[1] Many theoretical questions arise on error production and the underlying mechanisms involved in error production, detection, and correction (see Postma, 2000, for a review). For instance, Schmidt and Gordon (1977) studied the cost and benefit of anticipated movement initiation. In the present article, we focus on the mechanism for movement initiation itself and discuss various alternatives for error production, that is, false movement initiation, and their implementation in terms of dynamical systems currently discussed in the literature.

To do so, we have to formalize as follows our definition of a false movement initiation (false start):

A system shall have the ability to perform a movement cycle as a consequence of a stimulus for a fixed set of parameters. If the system performs the same movement cycle, or partially executed forms thereof, in the absence of the external signal, then we call the movement cycle a false start.

That definition of a false start implies its probabilistic character and, hence, is dependent on the presence and strength of fluctuations, which are always present in real dissipative systems (Haken, 1983). The notion of intention does not explicitly occur in our definition, but it is implicitly present as a

variable that changes the likelihood of a false start. Our definition provides a minimal basis, which enables us to study some characteristic properties of false starts but certainly is not intended to capture all aspects of a false start presented in the literature.

Given the above formalization of a false start, what are its possible realizations in dynamic systems? In Schöner's (1990) two-dimensional model, the system initiates a discrete movement by "turning on" a "behavioral information" just long enough to get a joint or limb from a given position A to another position B in phase space. The phase space is spanned by two variables, x and y. Here, x may be interpreted as the position of an effector and y as a variable that is related to the velocity. The behavioral information changes the phase flow topology temporarily from a structure with two stable fixed points A and B (see Figure 1a) to a limit cycle (see Figure 1c). Figure 1 shows a graphical representation of such trajectories with varying phase flow topologies. If the behavioral information does not remain "on" long enough, then the system will return to point A; if it stays on too long, then the system actually passes point B and also returns to point A, but performs a large amplitude flexion–extension cycle first (see Figure 1b). It appears that most of the complexity of the formation of movement trajectories has been shifted into the creation of behavioral information. In particular, the occurrence of false starts raises the question of how a whole movement cycle is initiated, even though the mover has no intention of doing so. Given the present formal definition, it seems reasonable to interpret the initiation of a false start as a stochastic process that operates close to a threshold: If the system crosses the threshold, for instance, as a result of a larger fluctuation, then the formation of the resulting trajectory will be dominated by its deterministic features. However, the onset of a false start will have a probabilistic character that will be a function of expectation and attentional factors, which should be directly correlated with the distance of the fixed point to the threshold in phase space for a fixed noise level. On the other hand, notice that the introduction of noise and variability into the concept of behavioral information, which is the cause of the movement initiation in Schöner's (1990) model, would result in a whole range of behaviors, from simple deviations around position A through half-cycles (AB), full cycles (ABA), and 3/2 cycles (ABAB). To narrow the range of behaviors to partial movement cycles, such as simple deviations around the fixed point, and complete movement cycles only (ABA), one would have to postulate that behavioral information occurs in a quantized manner, such that it may fluctuate only within specified time windows. Such a requirement not only seems artificial; in addition, it merely shifts the initial question of why either no movement or a complete movement is initiated to the alternative question of why either no behavioral information or behavioral information that lasts only for a specific time window is generated.

For those reasons, we chose to remain in the original two-dimensional phase space spanned by the variables x and y and to discuss which elements must be present so that one would observe the aforementioned phenomena of false starts, rhythmic and discrete movements, and shape of phase space trajectories. One may need additional degrees of freedom, as has been shown by Beek et al. (2002), to capture lag-one correlation effects (Wing & Kristofferson, 1973). Lower dimensional systems may still capture such dynamics satisfactorily as long as the dynamics is not chaotic, because deterministic chaos requires at least three degrees of freedom (Strogatz, 1994). One can accomplish that by identifying the two-dimensional phase space in x and y with a two-dimensional attractive surface in a higher dimensional space. As a consequence, any deviation from that surface will result in a dynamics back to the surface that satisfies the criteria of Beek et al. However, the dynamics is reducible to a two-dimensional dynamics (if, for instance, one uses techniques such as the order-parameter concept of synergetics [Haken, 1983]). We chose to focus primarily on the existence of topological structures (e.g., layout of fixed points, limit cycles) rather than on details of phase space trajectories. Separatrices are examples of topological structures; they partition the phase space locally into separate regimes. A well-known example in a one-dimensional phase space is the unstable fixed point of the HKB potential in bimanual coordination (Haken et al., 1985) separating the two stable fixed points, in-phase and antiphase. Homeomorphisms are smooth continuous transformations from one set of variables to another that preserve the topology of the flow in phase space. Hence, to achieve a classification of dynamic sys-

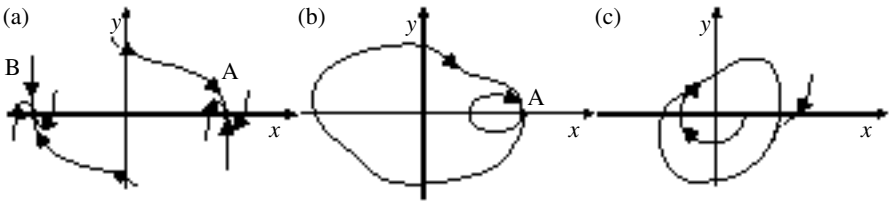

FIGURE 1. Topological features of phase flow: (**a**) Two stable fixed points A and B. (**b**) One stable fixed point A displaying either small-amplitude deviations or large-amplitude orbits. (**c**) Stable limit cycle. x and y are variables (such as position and velocity) in the two-dimensional phase space.

tems, it is sufficient for us to discuss the properties of one specific system only if we are able to find a homeomorphism that maps the particular system onto a class of other systems. In fact, the class of systems will actually be defined by the specific system and the homeomorphism. We present examples of those later on.

Our starting point in the modeling is the following: We need at least one stable fixed point in phase space, which will represent our rest position A as shown in Figure 2. Second, we need some kind of barrier or threshold near that fixed point such that on one side of the barrier the flow in phase space is directed toward the fixed point, on the other side away from it. That is accomplished by means of a separatrix, which divides the local neighborhood into two distinct areas with opposite horizontal flows (see Figure 2).

The separatrix introduces naturally the threshold-like properties of a false start. The existence of a separatrix is the basis for the current model. More generally, a nullcline is the graphical representation of the set of points for which either the horizontal or the vertical flow is zero. The intersection of two nullclines identifies fixed points, that is, points with zero horizontal and vertical flow in phase space. Without loss of generality we choose the separatrix as $y = -x$, which is identical to the nullcline of the horizontal flow. The sign of the flow must be chosen to be repelling, that is,

$$\dot{x} = x + y - g_1(x), \tag{1}$$

where $g_1(x)$ is a purely nonlinear function, $\partial_x g_1 = 0$ for $x = 0$, and guarantees that the trajectories remain bounded horizontally, if $g_1(x \to \pm\infty) \to \pm\infty$. In our notation, the dot is the derivative with respect to time and ∂_x is the derivative with respect to x. A slightly stronger condition is the requirement of point symmetry, $g_1(-x) \xrightarrow{x\to\pm\infty} -g_1(x)$, which also guarantees boundedness. Note that the previous condition is sufficient; however, because a point-symmetric function g_1 is often used in applications, we will use that constraint unless stated otherwise. The nullcline of the vertical flow $\dot{y}$ must generate at least one fixed point (x_0, y_0) at position A in phase space, $\dot{y} = f(x_0, y_0) = 0$, which is given by the intersection of the nullclines of horizontal and vertical flow. To guarantee linear stability of the fixed point, we require for the vertical flow

$$\dot{y} = f(x,y) = \underbrace{f(x_0,y_0)}_{=0} + \underbrace{\partial_x f(x_0,y_0)}_{\le 0}(x - x_0) + \underbrace{\partial_y f(x_0,y_0)}_{\le 0}(y - y_0) + \text{higher orders}. \tag{2}$$

We identify $\partial_x f(x_0, y_0) = -1$, $x_0 = a$, and $g_2(x, y) = -\partial_y f(x_0, y_0)(y - y_0) + O(x^2, y^2)$, where $O(x^2, y^2)$ is the Landau symbol, which means that it contains polynomials of at least the second (or higher) order. With those considerations we obtain the following ordinary differential equations,

$$\begin{aligned} \dot{x} &= [x + y - g_1(x)]\tau, \\ \dot{y} &= -[x - a + g_2(x, y) - I]/\tau, \end{aligned} \tag{3}$$

where τ is a time constant and external input I is introduced via the vertical flow. The model system in Equation 3 falls into the class of excitable systems, that is, systems that exhibit threshold properties and return, when having crossed the threshold, to the initial position after a long transient for an appropriate choice of $g_1(x)$ and $g_2(x, y)$. Excitable systems[2] have been studied in various fields of science dealing with threshold elements (Strogatz, 1994), particularly in biology, as a model for neuronal functioning (Murray, 1993). In the following, we refer to the model system described in Equation 3 as the *excitator*. To ensure the excitable properties of Equation 3, the model has to satisfy the following constraints, which are derived in the Appendix:

Existence of a separatrix: $\partial_x g_1(0) = 0$,

Stability of fixed point (x_0, y_0):

$$\partial_x g_1 > 1, \qquad \partial_y g_2(\partial_x g_1 - 1) + \partial_x g_2 + 1 \ge 0,$$

Boundedness $(x, y \gg 1)$:

$$g_1(-x) \xrightarrow{x\to\pm\infty} -g_1(x) \quad G(-y) \xrightarrow{y\to\pm\infty} -G(y)$$

$$G(y) = g_1^{-1}(y) - a + g_2[g_1^{-1}(y), y], \tag{4}$$

where the partial differentials in the constraint for the stability of the fixed point (x_0, y_0) have to be evaluated at the fixed point. One should choose the time constant τ to be large, $\tau \gg 1$, to guarantee sufficiently fast horizontal flow away from the separatrix. Actually, in practice, it turns out that $\tau \ge 1$ is fully sufficient. Under those conditions, x becomes a fast variable and y becomes a slow variable, resulting in a sequentially occurring time scale hierarchy. Such systems are referred to in the literature as *relaxation oscillators*—for example, the FitzHugh–Nagumo system (FitzHugh, 1961), the Hodgkin–Huxley equations (Hodgkin & Huxley, 1952), the Hindmarsh–Rose oscillator (Hindmarsh & Rose, 1982), and the Van der Pol oscillator (see, e.g., Perko, 1991).

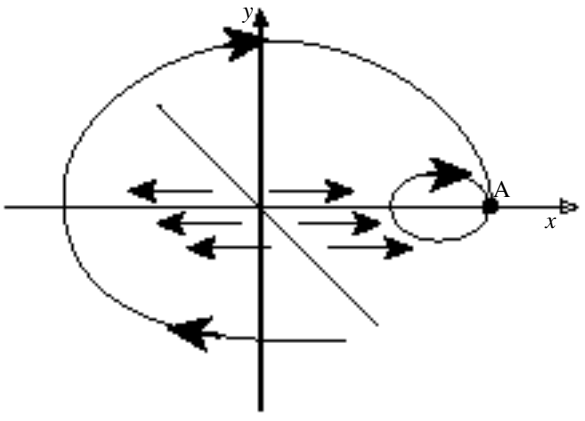

FIGURE 2. A separatrix divides the phase flow locally into two separate regimes located to its left and right, thereby creating a threshold element and thus the propensity to false starts. The direction of flow is indicated by arrows.

Those dynamic systems typically have a parameter regime in which there is limit cycle behavior. One can demonstrate that behavior by applying the Poincaré–Bendixson theorem (e.g., Haken, 1983); according to that theorem, there is a stable limit cycle if a closed region may be found in the phase space, such that the flow at the boundaries of the region points inside and the region does not contain any fixed points. The boundedness criterion of Equation 4 guarantees an outer boundary with inward flow. An inner boundary, its flow, and the fixed points will depend on the details of the functions $g_1(x)$, $g_2(x, y)$. The primary purpose of $g_1(x)$ is to guarantee the boundedness of the system dynamics along the x direction, whereas $g_2(x, y)$ identifies the task conditions. In particular, we will use the expression $-a + g_2(x, y)$ to implement the task constraints (see the following for explicit examples) reflected in the topology of the phase flow.

A notable feature of the phase plane trajectories is that the sequential time scale hierarchy, x being a faster variable than y, creates an attractive manifold in phase space if the system is sufficiently far away from the separatrix. In that region, the different time scales allow one to eliminate the fast variable x by means of adiabatic elimination (Haken, 1983), $\dot{x} = 0$. We thereby obtain a reduced description of the dynamics,

$$y \approx g_1(x) \tag{5}$$

and

$$\dot{y} = -\{g_1^{-1}(y) - a + g_2[g_1^{-1}(y), y] - I\}/\tau, \tag{6}$$

as long as the system dwells in that region of phase space. Along this "return manifold," the trajectory returns from an overshoot and moves toward a stable fixed point or just defines a segment on the left- and right-hand sides of the limit cycle in phase space (see the next section for illustrations). The inverse of $g_1(x)$ must exist only locally in phase space, that is, in the region of interest. Experimental and theoretical examples are presented in the next section.

A simple realization of the excitator, which satisfies all conditions in Equation 4, is given by $g_1(x) = x^3/3$ and results in the following dynamic system:

$$\begin{aligned} \dot{x} &= (x + y - 1/3x^3)\tau, \\ \dot{y} &= -(x - a + by - I)/\tau, \end{aligned} \tag{7}$$

where the three task conditions are defined by the parameters a and b: Condition 1, bistable ($a = 0$, $b = 2$); Condition 2, monostable ($a = 1.05$, $b = 0$); Condition 3, limit cycle ($a = 0$, $b = 0$). The nullclines of the two-dimensional flow, $y = -x + (1/3)x^3$ for the horizontal flow and $x = a - g^2(x, y)$ for the vertical flow, are plotted in Figure 3 for the three different conditions. The intersections of the nullclines define the stable and unstable fixed points.

The monostable condition displays exactly one fixed point $(a, -a + a^3/3)$. A linear stability analysis shows immediately that the fixed point is stable for $| a | > 1$, else unstable. As a consequence, there will be a stable limit cycle for $| a | < 1$ because there are no other fixed points and the Poincaré–Bendixson theorem applies. We illustrate the results of the stability analysis in Figure 4 by means of a bifurcation diagram. The excitator undergoes a supercritical Hopf bifurcation at $| a | = 1$.

Note the difference from the previously discussed equilibrium-point notions (Feldman, 1980a, 1980b; Kelso, 1977; Polit & Bizzi, 1978, 1979). Equilibrium-point models accomplish movement control by changing the location of an unambiguous fixed point within the location of the phase plane. As a consequence, they do not describe phenomena such as limit cycles or the existence of multiple stable fixed points. In that sense, the equilibrium models may be viewed as a special case of the excitator system. Obviously, we acknowledge that the equilibrium-point models have the benefit of making the connection to the underlying biomechanical aspects of movement control.

Trajectory Formation in Phase Space: Experiment and Computation

The set of variables x and y provides a complete description of the dynamics of a two-dimensional excitable system. Here we use a convention most often used in the context of excitable systems (Murray, 1993; Strogatz, 1994). That convention separates the time scales present in the dynamics, that is, a fast time scale on the order $1/\tau$ associated with the x variable and a slow time scale on the order of τ associated with the y variable. That clear time scale separation enables us to formulate an unambiguous criterion for the separatrix—that is, sufficiently fast horizontal flow away from the separatix with $\tau \gg 1$. The fixed points are obtained from the intersections of the nullclines and may be located anywhere in phase space. On the other hand, it is experimental practice to identify the second variable with the effector velocity, $y = \dot{x} = \partial_t x$. As a consequence, all fixed points are located along the horizontal x-axis. From Equation 3, it is evident, however, that the second y variable is not the effector velocity $\dot{x}$ but instead is a nonlinear function of x and $\dot{x}$, that is, $y = \dot{x}/\tau - x + g_1(x)$. To perform a comparison between experimental and theoretical results, we have to identify a mapping between the two coordinate systems used in experiment and theory. In particular, we map the theoretical set of variables x, y onto a new set of variables, u, v. The new set of variables is required to satisfy the condition $v = \dot{u}$. If the mapping is a homeomorphism, then the dynamics will remain the same in both coordinate systems; that is, the mapping does not alter the topology of the phase flow. In general, we will use x, y for discussing the intrinsic dynamics of the excitator in Equation 3 and u, v for comparison with the experimental system.

We seek a mapping $h_1(x)$, $h_2(x, y)$ such that

$$\begin{aligned} u &= h_1(x) = x, \\ v &= h_2(x, y), \end{aligned} \tag{8}$$

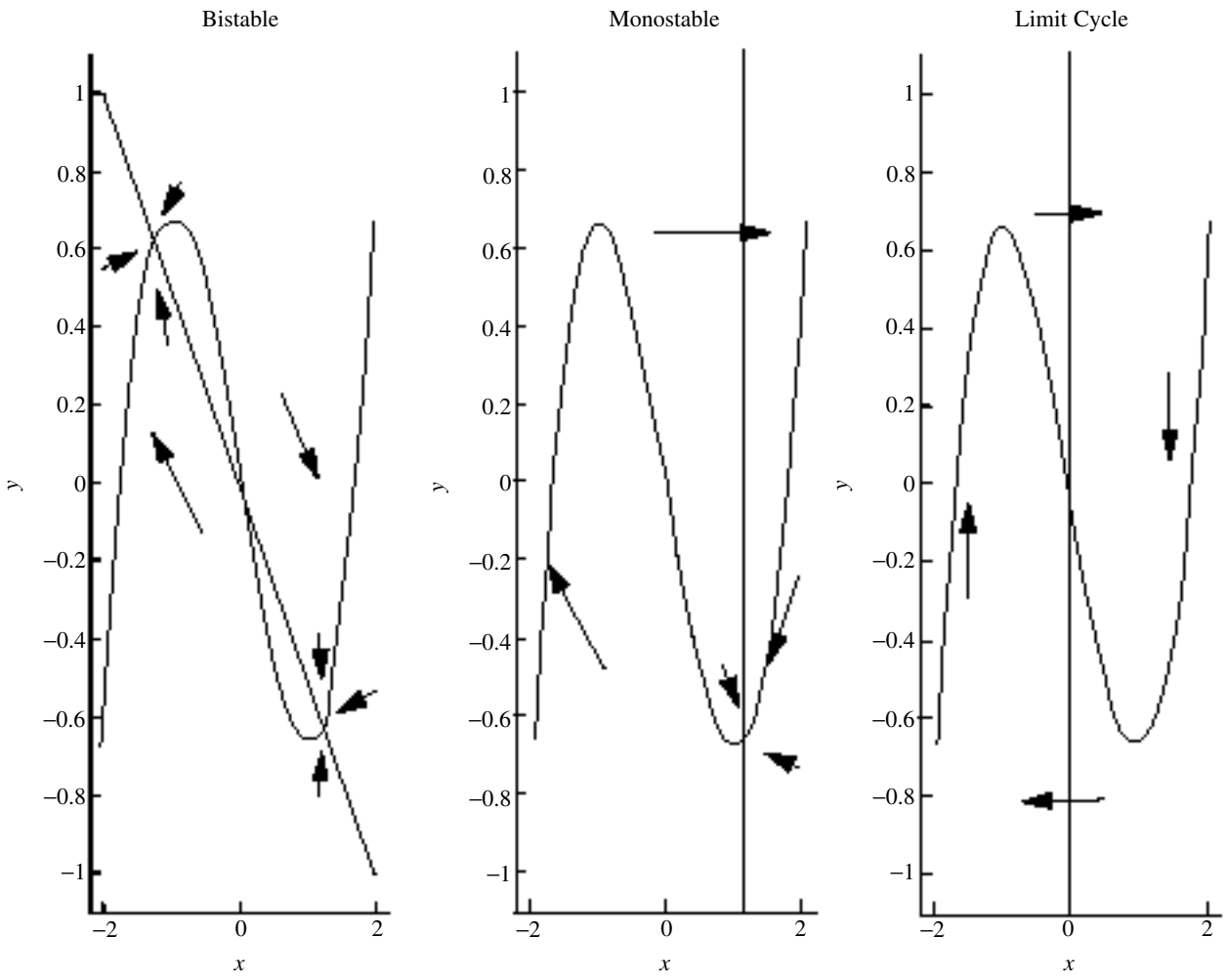

FIGURE 3. The nullclines for the three conditions, bistable, monostable, and limit cycle, are plotted together with arrows indicating the direction of the flow in the phase space. The cubic curve is the nullcline for $\dot{x} = 0$ and remains unchanged; only the $\dot{y} = 0$ nullcline is altered; so, one can define the task conditions by adjusting the flow and topology in phase space.

where the new variables u, v satisfy with Equation 3

$$\dot{u} = v = h_2(x, y) = (\partial_x h_1)\dot{x} = [x + y - g_1(x)]\tau, \text{ and } \partial_x h_1 = 1. \quad (9)$$

Here h_1 and h_2 are differentiable and smooth over x, y and, hence, will not alter the topology of the phase flow in the new coordinates u, v. Then, the mapping from (x, y) to (u, v) coordinates and its inverse are given by

$$\begin{aligned} u &= x & x &= u \\ v &= [x + y - g_1(x)]\tau & y &= v/\tau - u + g_1(u). \end{aligned} \quad (10)$$

The dynamics of u, v may be readily written as

$$\begin{aligned} \dot{u} &= v, \\ \dot{v} &= (\partial_x h_2)\dot{x} + (\partial_y h_2)\dot{y}, \\ &= (1 - \underbrace{\partial_x g_1(x)\big|_{x=u}}_{\gamma_1(u)})\tau v - u - g_2(u, v) + a + I, \end{aligned} \quad (11)$$

where $g_2(u, v) = g_2[u, y(u, v)]$. It is fully equivalent to either solve Equation 3 and then map x, y onto u, v or, alternatively, perform the numerical solution directly in Equation 11. The specific realization of the excitator given in Equation 7 reads in u, v coordinates as follows:

$$\begin{aligned} \dot{u} &= v, \\ \dot{v} &= (1 - u^2)\tau v - u - b(v/\tau - u + 1/3u^3) + a + I. \end{aligned} \quad (12)$$

It is evident that the time scales of evolution are mixed in Equation 12, whereas they are unmixed in Equation 7.

Method

We briefly present experimental data. Our primary purpose here is to illustrate characteristic features of phase plane trajectories; our secondary purpose is to identify space and time scales that will allow us to identify parameters in specific realizations of excitator models (see the following). Ten self-reported, right-handed men took part in this experiment. The local Human Subjects Committee

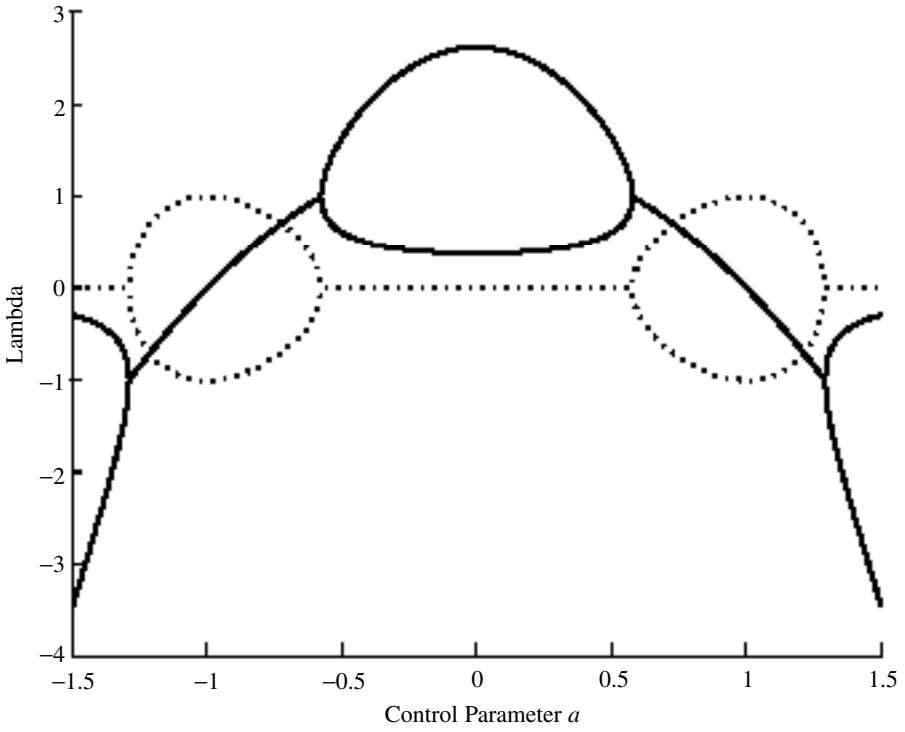

FIGURE 4. Bifurcation diagram. The real parts (solid line) and the imaginary parts (dotted line) of the eigenvalue of the linear stability analysis around the fixed point A are plotted in this bifurcation diagram. A supercritical Hopf-bifurcation occurs at $|a| = 1$.

cleared all procedures, and participants signed consent forms before taking part in the experiment.

Participants placed the index finger of their dominant hand in a custom-built manipulandum that restricted motion of the metacarpophalangeal joint to a single plane (see Kelso & Holt, 1980, for more details about the apparatus). We restricted unnecessary vertical and horizontal movements by means of a padding placed against the sides of the hand. An angle-calibrated potentiometer measured the position of the index finger. We sampled finger movement at 128 Hz by using an Optotrak ODAU analog–digital converter (Northern Digital, Inc., Waterloo, Ontario, Canada) connected to an Optotrak 3010 system. The external metronome, consisting of a sequence of beeps, was sent to the ODAU and to a pair of headphones. We tested three experimental conditions: (1) the bistable condition, in which there are two fixed points; (2) the monostable condition, which exhibits only one fixed point; and (3) the limit cycle condition. In the first two conditions, we exposed participants to a sequence of auditory stimuli of 30-ms duration and variable interstimulus intervals (4,000 ±1,000 ms), and we instructed them to react to the stimuli as quickly as possible. In Condition 1, the participants' task was to alternate between the execution of flexion and extension. In Condition 2, the participants' task was to perform a complete flexion–extension cycle and return to the initial starting point. In the last condition (3), we presented periodic stimuli of 30-ms duration with an interstimulus interval of 1,000 ms. The participants' task was to perform continuous periodic movements, coinciding peak flexion with stimulus onset.

For the computational implementation of all simulations in The Intrinsic Dynamics of the Excitator section of this article, we chose the following specific realization of the excitator system:

$$\begin{aligned} \dot{x} &= \left[x + y - \left(\frac{1}{3}x^3 + \frac{1}{5}x^5 \right) \right] \tau, \\ \dot{y} &= -(x - a + by - I) / \tau, \end{aligned} \tag{13}$$

with $\tau = 1$, $g_1(x) = (1/3)x^3 + (1/5)x^5$, and $g_2(x, y) = by$. We obtained the function $g_1(x)$ from a fit of the nullcline $y = -x + g_1(x) = -x + (c_1/3)x^3 + (c_2/5)x^5$ to the experimental data in the neighborhood of the two fixed points of the bistable condition. We used the data set of a single characteristic participant for the parameter fit. The other conditions (monostable and limit cycle) and data sets of other participants provided similar results. We determined the parameters $c_1 \approx c_2 \approx 1$ to minimize the square error of the curvature of the stable manifolds but also to provide computationally stable solutions for all task conditions discussed in the current section. The task conditions are implemented in the term $-a + g_2(x, y) = -a + by$, with a, b varying between 0 and 2. We chose the parameters a and b to mimic the location of the fixed points in the experimental data set of the corresponding task condition. Input

strength was $I = 1$ for the on periods of the stimuli; otherwise $I = 0$. For the monostable condition, the input I was defined to be positive for each stimulus. For the bistable condition, the sign of I alternates between plus and minus. For the limit cycle condition, no input is provided; that is, $I = 0$ throughout. The duration of the rectangular stimulus I was one computational time unit. We performed all simulations by using a fourth-order Runge–Kutta method. We also added Gaussian white noise $\xi(t)$ to the evolution equations, where

$$<\xi(t)> = 0, \quad <\xi(t)\xi(\tau)> = Q^2\delta(t - \tau), \quad Q = 0.01. \quad (14)$$

The triangular brackets (< and >) denote time averages. We estimated the relation between the computational units and the corresponding physical units in meters and seconds. One computational space unit corresponded to 2 cm, estimated from the radius of the limit cycle in phase space and put in correspondence with average experimental limit cycle data. The estimate also provided a good comparison between experiment and theory for the distance of the positions of the two fixed points in the bistable condition. The time unit estimate was based on the choice for the computational angular eigenfrequency $\omega = 2\pi f = 1/T = 1$ of the excitators (see Equation 12), where f is the frequency and T the period of a cycle. Experimentally, preferred finger movement frequencies range from around 1.1 Hz to 3.0 Hz following instructions to move the finger at a comfortable pace and through a comfortable range of motion (Fink, January 8, 2002, personal communication). If we identify the preferred frequency with the eigenfrequency and estimate it as 2 Hz, then one computational time unit will correspond to 80 ms or, equivalently, 12.5 computational time units will correspond to 1 s. In the following, we based all theoretical predictions on those estimates.

Results

We compared representative examples of time series and phase space trajectories of experimental and simulated data. The first condition was the bistable condition, in which a participant had to move the index finger from a position A to a position B coincident with a metronome beat. Figure 5 displays both experimental (left column) and simulated (right column) data. In the top panel, the time series of the end-effectors are shown for a few repetitions, together with the corresponding stimulus sequence. Below, the phase space trajectories are plotted in u, v coordinates (middle panel) and x, y coordinates (bottom panel). More repetitions have been plotted in the bottom panel than in the top panel for reasons of clarity. In both data sets, the fixed points are identified on the

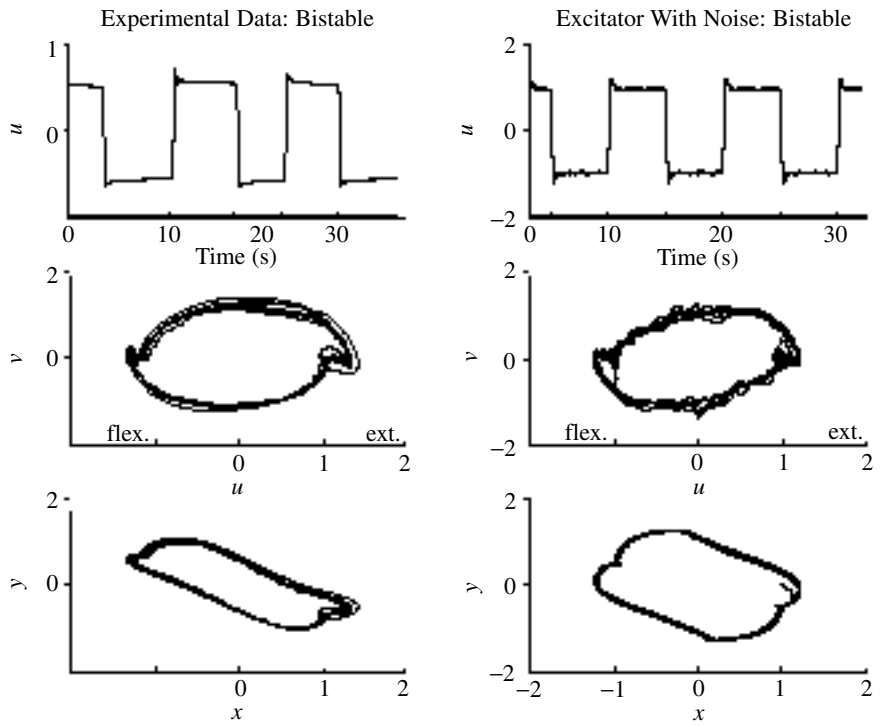

FIGURE 5. Two fixed points A and B were created in phase space. The left column shows experimental data, the right column numerical simulations. The time units are in seconds; the space units are dimensionless. The phase space trajectories are represented in the u, v coordinate system (middle panel), which ensures that the fixed points are located along the horizontal axis in phase space, as well as in the x, y coordinate system (lower panel). The mapping given in Equation 10 has been used with $\tau = 1$ and $g_1(x) = x^3/3$. flex. = flexion; ext. = extension.

horizontal axis ($v = 0$) as clustering points. Note that both experimental and simulated time series displayed an overshoot when they approached the fixed point and stabilized there. The overshoot corresponded to the movement along the return manifold discussed earlier in the section on Trajectory Formation in Phase Space: Theory. In the u, v system (middle panel), that motion evolves along $v = 0$ by construction, whereas in the x, y system (lower panel), the motion follows a concave curve leading to the fixed points. The mapping from u, v coordinates to x, y coordinates is defined by Equation 10 with $\tau = 1$ and $g_1(x) = x^3/3$. In the following, we use the u, v coordinates, which may be identified with the commonly used variables position and velocity.

The monostable condition displays one fixed point and a flexion–extension cycle when the fixed point is destabilized. We have plotted the experimental data (left column) and simulated (right column) data in Figure 6 by using u, v coordinates. The phase space trajectories display the fixed point on the right side of the trajectories as clear clustering points. Two of the movement cycles are plotted in the top panel. Here, we note again the overshoot that occurred after the execution of a flexion–extension cycle.

The overshoot and the slow fall-off toward the rest state correspond to the motion along the return manifold. The arrows in Figure 6 point toward the attractive manifolds around $v = 0$. In analogy to refractory times of neurons (FitzHugh, 1961; Hindmarsh & Rose, 1982; Hodgkin & Huxley, 1952), the return phase of the movement cycle along the manifold corresponds to the refractory part of the dynamics, in which the system is more difficult to excite, and lasts until the fixed point is reached. Using the parameter identification in the Method section, we estimated the movement time to be on the order of 400 ms, defined from movement onset to the maximum value of extension (that is, maximum positive u). At the latter point, the return phase of the movement cycle started and also lasted for about 400 ms in both experimental and theoretical data sets. However, the movement onsets of the theoretical data were instantaneous at stimulus onset. The experimental data set shows the well-known delay between stimulus and movement onset, which is sensory-modality dependent and is attributed to perceptual processes (Hackley & Valle-Inclán, 1998).

In Figure 7, the experimental (left column) and simulated (right column) data of the limit cycle condition are displayed in u, v coordinates. The simulated trajectories appear to be more symmetric than the experimental trajectories with respect to point symmetry. Both data sets show structures that are reminiscent of the return manifolds in the neighbor-

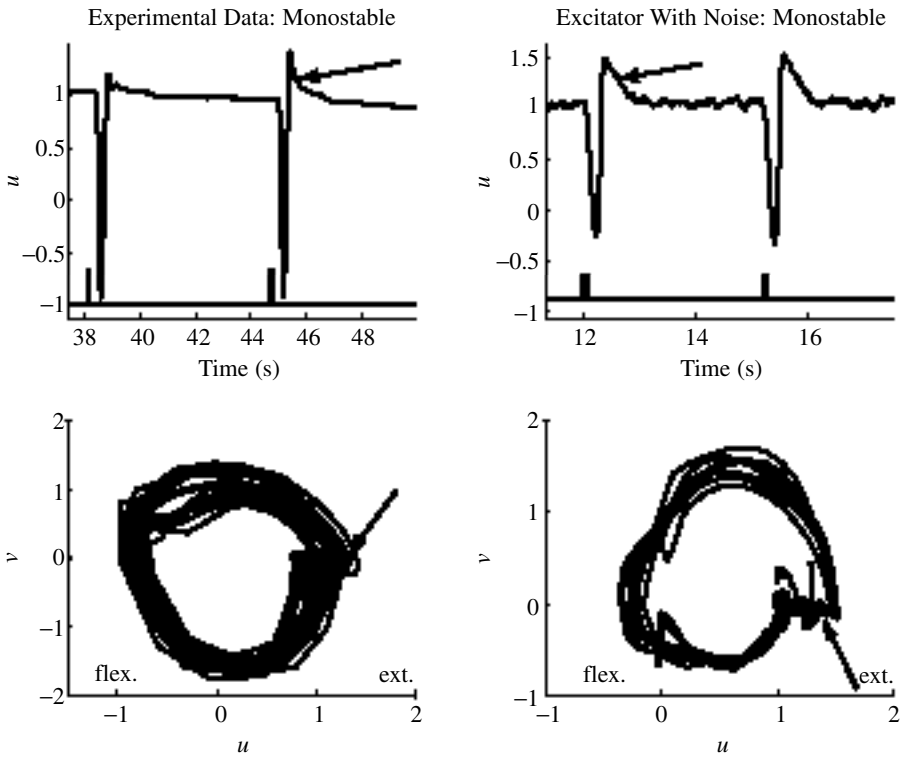

FIGURE 6. One fixed point A is created in phase space. The left column shows experimental data, the right column displays the results of the numerical simulations. The time units are in seconds; the space units are dimensionless. Both data sets are represented in the u, v coordinate system. The dynamics along the attractive return manifolds, $v \approx 0$, is indicated by arrows in the time series and the phase spaces. The time series of the stimulus signal is also plotted in the upper graph. flex. = flexion; ext. = extension.

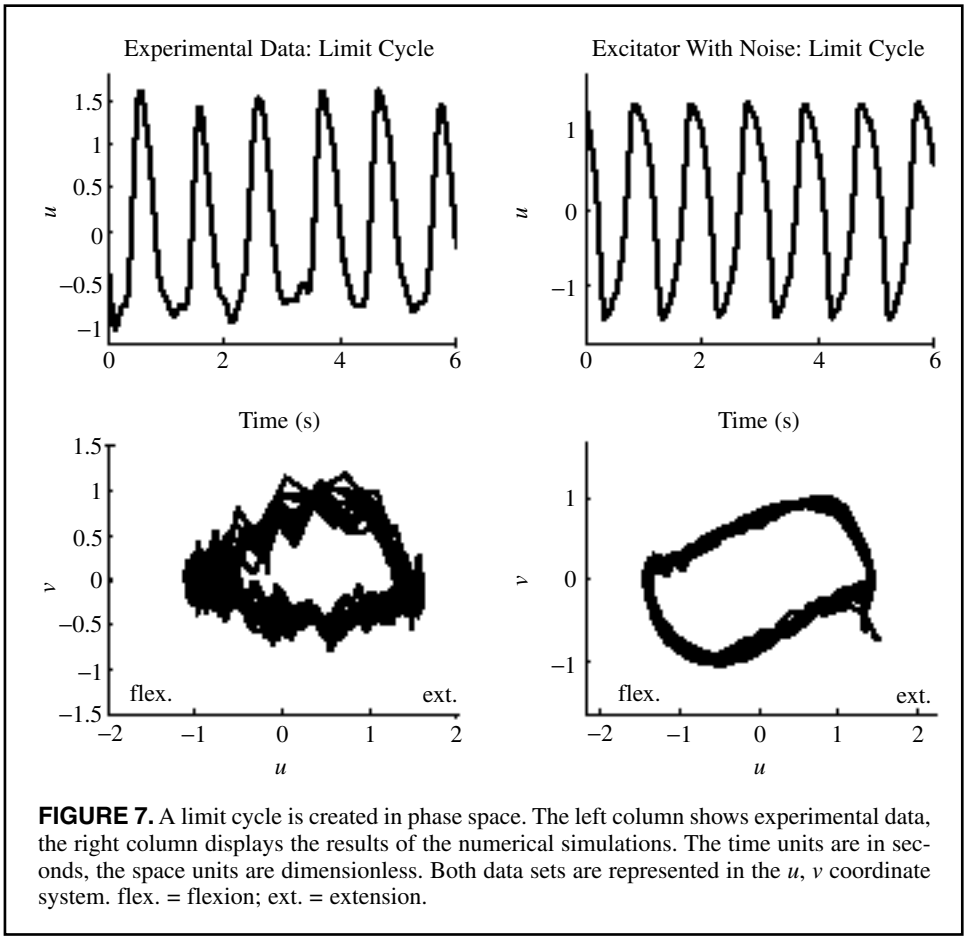

FIGURE 7. A limit cycle is created in phase space. The left column shows experimental data, the right column displays the results of the numerical simulations. The time units are in seconds, the space units are dimensionless. Both data sets are represented in the u, v coordinate system. flex. = flexion; ext. = extension.

hood of $| u | \approx 1$, such that the deviations from the circular structure of the trajectories are more pronounced in those regions and a higher clustering of data points occurs.

Coupled Dynamics of Two Excitators

The phenomenon of in-phase and antiphase behavior of two coupled oscillating systems is omnipresent in nature. It has received particular attention in movement science (for reviews, see Jirsa & Kelso, 2004; Kelso, 1995) because of its simplistic nature, that is, the reduction of its degrees of freedom: By forcing the effectors of the human movement system onto limit cycles, which one typically does by providing adequate task conditions, the phases of the effectors become the collective variables carrying the relevant movement information. Kelso (2002) provided a general discussion of the dynamics observable in a system described by a phase equation. In particular, he pointed out that there are coexisting integrative (converging) and segregative (diverging) tendencies in the proximity of fixed points. Kuramoto (1984) has shown that any two weakly coupled oscillators, whose limit cycle properties are preserved despite the coupling, may be reduced to a system of coupled phase equations. The stationary solutions of the phases are always the in-phase and antiphase solutions. The stability of those solutions is determined by the details of the coupling. The constraint of limit cycle oscillators enabled Kuramoto to draw conclusions about a variety of oscillators. Here, we dropped that constraint of limit cycle behavior. Instead, we allowed arbitrary trajectories in a two-dimensional phase space but constrained the nature of the coupling. Sigmoidal nonlinearities represent the most natural form of coupling in biological systems for the following reason: A population of cells without any afferent input displays only background rest activity. When the input to the cell population is increased, there is typically an initial linear increase of cell activity. At some point, the cell population will reach its maximal activity possible, and the response function saturates, resulting in a sigmoidal response curve. Multimodal response curves for increasing input, such that the response of the cell population decreases and increases again, will be unlikely because those are subject to averaging out in a cell population. However, nonmonotonic behavior of neuronal firing rates has also been observed for large inputs to the neuron, reflecting properties of fatigue and adaptation (Freeman, 1992). In the movement sciences, the HKB coupling (Haken et al., 1985) has been successful in enabling researchers to understand a number of coordination phenomena on the limit cycle. That coupling function consists of a linear polynomial with a positive coefficient and a cubic polynomial with a negative coefficient. The sign and magnitude of the coefficients are determined by the stability properties observed in bimanual rhythmic coordination

behavior (Haken et al., 1985; Schöner, Haken, & Kelso, 1986). It turns out that those coefficients are the same as those for the low-order approximation of the sigmoid function (Jirsa et al., 1998), suggesting an interpretation of the HKB coupling as a truncated sigmoid function. If the latter is true, then the well-known dependence of the neural response functions on fatigue and attention (Freeman, 1992) may be transferred to the HKB coupling and to the movement sciences. In the following, we assume a sigmoidal coupling S between two excitator units and discuss the effects of the coupling on a variety of movement types, including rhythmic and discrete movements produced by the excitators. Whenever appropriate, we note the effects of the truncation resulting from the HKB coupling.

As a starting point, we choose two excitators described by the two sets of variables u_1, v_1 and u_2, v_2 with the intrinsic dynamics given by Equation 11. We keep the analytical discussion more general in the sense that our following results will also be valid for intrinsic dynamics other than the excitators. When appropriate, we note that the results are specific for excitators. The coupled system of two excitators then reads

$$\begin{aligned}\dot{u}_1 &= v_1,\\ \dot{v}_1 &= -u_1 + f_1(u_1, v_1) - \partial_t S(u_1 - u_2),\\ \dot{u}_2 &= v_2,\\ \dot{v}_2 &= -u_2 + f_2(u_2, v_2) - \partial_t S(u_2 - u_1),\end{aligned} \tag{15}$$

where f_1 and f_2 denote the intrinsic dynamics of the dynamic systems involved, for example, an excitator dynamics. For the time being, we wish to keep the specific realization of the intrinsic dynamics open. The HKB coupling is obtained as a truncation of the expansion of the sigmoid after its second term

$$\begin{aligned}\partial_t S(u_1 - u_2) &= (\dot{u}_1 - \dot{u}_2)\partial_u S(u)\\ &= (v_1 - v_2)[\alpha + \beta(u_1 - u_2)^2 + \ldots]\\ &\approx (v_1 - v_2)[\alpha + \beta(u_1 - u_2)^2],\end{aligned} \tag{16}$$

with α, β as constant parameters. To investigate the behavior of the excitators with respect to each other, we study the evolution of their relative distance in phase space. The Euclidean distance of two excitators in phase space is given by $d = [(u_1 - u_2)^2 + (v_1 - v_2)^2]^{1/2}$ (see Figure 8), and it evolves in time as

$$\begin{aligned}\partial_t d &= (v_1 - v_2)[(u_1 - u_2) + (\dot{v}_1 - \dot{v}_2)] / d\\ &= (v_1 - v_2) / d[\underbrace{f_1(u_1, v_1) - f_2(u_2, v_2)}_{\Delta}\\ &\quad -\partial_t S(u_1 - u_2) + \partial_t S(u_2 - u_1)]\\ &= (v_1 - v_2) / d \times \Delta - 2\underbrace{(v_1 - v_2)^2 / d}_{>0} \times \underbrace{\partial_u S(u_1 - u_2)}_{<0 \text{or} >0}.\end{aligned} \tag{17}$$

The behavior of the trajectories in phase space is then given by

$$\begin{aligned}&\text{convergence} \quad \leftrightarrow \quad \partial_t d < 0,\\ &\text{divergence} \quad \leftrightarrow \quad \partial_t d > 0.\end{aligned} \tag{18}$$

Let us assume for a moment that the difference in the individual dynamics is $\Delta = 0$. Then convergence is obtained if and only if

$$\text{convergence: } \partial_t d < 0 \quad \leftrightarrow \quad \partial_u S(u_1 - u_2) > 0, \tag{19}$$

which is always satisfied for a unimodal sigmoid function. Hence, two sufficiently similar trajectories will always converge. In contrast, the partial derivative of the truncated sigmoidal function, $\partial_u S(u_1 - u_2) \approx \alpha + \beta(u_1 - u_2)^2$, allows also for divergence; that is,

$$\text{convergence: } \partial_t d < 0 \quad \leftrightarrow \quad \alpha + \beta(u_1 - u_2)^2 > 0, \tag{20}$$

and

$$\text{divergence: } \partial_t d > 0 \quad \leftrightarrow \quad \alpha + \beta(u_1 - u_2)^2 < 0. \tag{21}$$

The conditions in Equations 20 and 21 contain the special case of the coupled limit cycle oscillators discussed in Haken et al. (1985). When one constrains the dynamics of two oscillators to a one-dimensional closed loop in phase space, the limit cycle, then the greatest distance between these two oscillators, becomes half of the length of the closed loop, which is identical to antiphase motion and is stable as long as the condition in Equation 21 is satisfied. That is illustrated qualitatively in Figure 9. As the amplitudes u_1, u_2 of the oscillators decrease with increasing movement frequency (Haken et al., 1985; Kay, Kelso, Saltzmann, & Schöner, 1987), the divergence condition cannot be satisfied anymore, and the oscillators bifurcate into in-phase motion, which is the smallest distance between two limit cycle oscillators and is always stable for $\alpha > 0$.

Schöner (1990) first observed numerically another special case of Equation 17 for discrete movement trajectories. Here, the simulation of two Gonzalez–Piro oscillators (Gonzalez & Piro, 1987), which were coupled by means of the HKB coupling, revealed the tendency to synchronize two movements when the movement onsets were sufficiently close. Otherwise, the tendency to sequentialize the move-

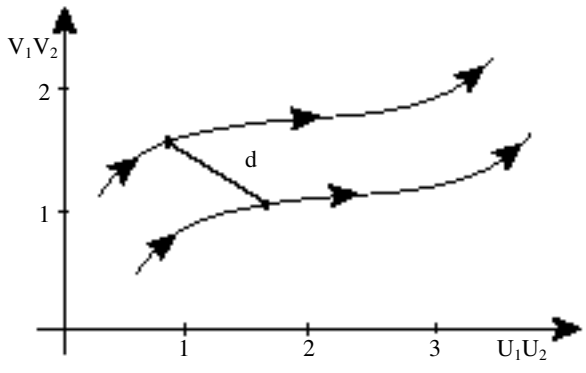

FIGURE 8. Two phase space trajectories are shown. The instantaneous Euclidean distance $d(t)$ in phase space is a measure of the similarity of two ongoing dynamics.

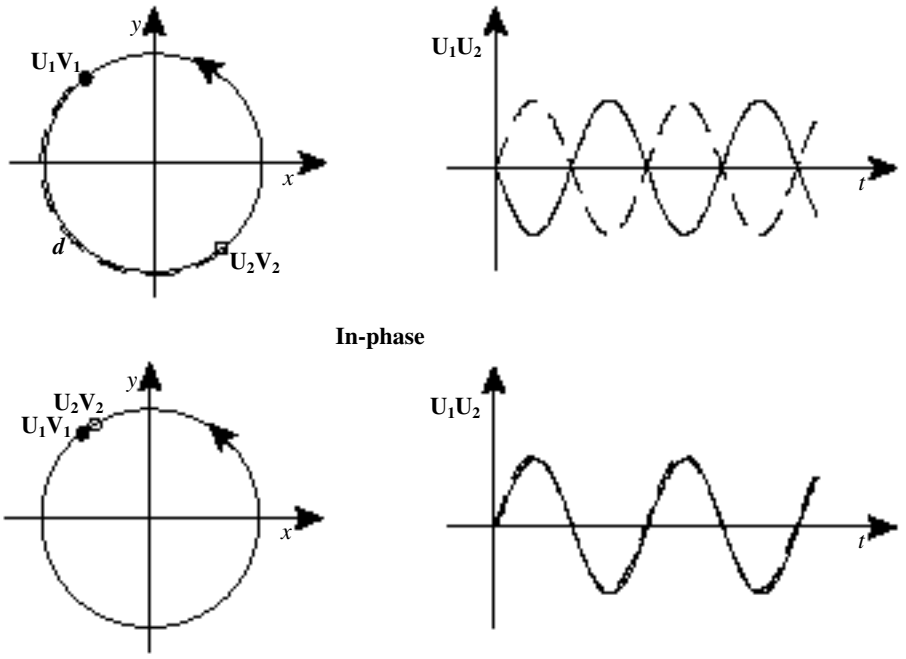

FIGURE 9. The Euclidean distance d of two limit cycle oscillators is maximal for antiphase motion as a consequence of divergent dynamics and is minimal for in-phase motion because of convergent dynamics.

ments was observed. We now may be more specific. It actually is not the movement onset times, but rather the difference in positions between the oscillators in Equations 20 and 21, that provides the critical value for convergence and divergence of trajectories.

The general case, $\Delta \neq 0$, introduces considerations on symmetry and similarity between the two movement trajectories. When two identical systems display the same trajectory formation, stationary or transient, then the resulting dynamics is determined solely by their mutual coupling and the earlier special case, $\Delta = 0$, is present. If the symmetry between the systems is broken—for example, if they have slightly different eigenfrequencies—then that will be reflected in Δ (for the special case of weakly coupled limit cycle oscillators, see Kelso, DelColle, & Schöner, 1990, and Kuramoto, 1984). Equivalently, if two identical systems take different paths in phase space, for example, slightly different positions, then that will also be reflected in Δ. We wish to identify now the intrinsic dynamics of the two coupled systems with the excitators in Equation 11 and write for the difference Δ of the intrinsic excitator dynamics

$$\Delta = \alpha_1 - \alpha_2 + [1 - \gamma_1(u_1)]\tau v_1 - [1 - \gamma_1(u_2)]\tau v_2 - g_2(u_1,v_1) + g_2(u_2,v_2), \qquad (22)$$

where $\gamma_1(u_i) = \partial_x g_1(x)\,|_{x=u_i}$. For a moment, we wish to refer back to the excitator system in Equation 3 in the x, y coordinates and use the convenient property of unmixing of the time scales in this coordinate system. In particular, there are two sequentially occurring separate time scales: that is, a fast horizontal flow and a slow dynamics around the outer branches (i.e., $x > a$) of the nullcline $y = x + g_1(x)$ (see, e.g., Campbell & Wang, 1998, for a technical review). Using Equation 10, the slow manifold reads $v = 0$ in u, v coordinates. During a stationary or transient dynamics, most of the time will be spent on this slow manifold in the phase space. Hence, we can make the following argument: Because $\gamma_1(u)$ is symmetric—that is, $\gamma_1(-u) = \gamma_1(u)$ for $u = u_1, u_2$—there will be a lower bound for the expression γ_1 for both excitators and both slow manifolds, such as

$$\gamma_1(u) \geq \gamma_1(a), \quad u = u_1, u_2;\ a = \min(a_1, a_2). \qquad (23)$$

That argument may be made for $\gamma_1(u_1)$, $\gamma_1(u_2)$ because of its symmetry property, but not for the coupling $S(u_1 - u_2)$, which depends on the difference of u_1, u_2. Then Δ may be approximated (for sufficiently large τ and thus time scale separation) as

$$\Delta \approx a_1 - a_2 + [1 - \gamma_1(a_1)]\tau(v_1 - v_2), \qquad (24)$$

and the time evolution of the trajectories' distance reads

$$\partial_t d = (v_1 - v_2)/d \times (a_1 - a_2) - 2\underbrace{(v_1 - v_2)^2/d}_{>0} \times \{\underbrace{[\gamma_1(a_1) - 1]\tau/2 + \partial_u S(u_1 - u_2)}_{<0 \text{ or } >0}\}. \qquad (25)$$

In particular, if the fixed points $(u_i, v_i) = (a_i, 0)$, $i = 1, 2$

are stable and the symmetry breaking is small, $| a_1 - a_2 | \ll 1$, then Equation 25 is a first good approximation of the time evolution of the distance of two nearby trajectories. The sign of the last term will be the relevant criterion deciding about convergence or divergence. The critical trajectory distance is then given by

$$d_c = |u_1 - u_2| = \sqrt{\frac{[\gamma_1(a) - 1]\tau / 2 + \alpha}{-\beta}}. \quad (26)$$

If $d > d_c$, then the trajectories will diverge; else, they will converge. In the following simulations, we test those predictions numerically.

The following simulations of the coupled excitators are based on the excitator model in Equation 13 and its space and time scales as established in the Method section. The coupling is the HKB coupling as determined in Haken et al. (1985; Schöner et al., 1986) and discussed in the context of neural response functions in Jirsa et al. (1998). The explicit equations read as follows in u, v coordinates:

$$\begin{aligned}
\dot{u}_1 &= v_1. \\
\dot{v}_1 &= (1 - u_1^2 - u_2^4)\tau v_1 - u_1 + a_1 + I_1 \\
&\quad -(v_1 - v_2)[\alpha + \beta(u_1 - u_2)^2]. \\
\dot{u}_2 &= v_2. \\
\dot{v}_2 &= (1 - u_2^2 - u_2^4)\tau v_2 - u_2 + a_2 + I_2 \\
&\quad -(v_2 - v_1)[\alpha + \beta(u_1 - u_2)^2]. \quad (27)
\end{aligned}$$

The parameters are $a_1 = a_2 = 1.05$, $\tau = 3$, $\alpha = 0.2$, and $\beta = -0.2$. The choice of parameters resembles the monostable task condition with a single fixed point. The amplitude of the input stimulus is $I = -3.5$, and its duration is 80 ms. As described in the Method section, we used a fourth-order Runge–Kutta method including a linear noise term for the numerical implementation. With those parameters, the critical trajectory distance in Equation 26 is estimated to be $d_c = 3.3$ in computational space units, which corresponds to about 6.5 cm and thus suggests the spatial scale of the convergence and divergence phenomena to be of the order of magnitude that is experimentally observable. The numerical simulations of the dynamics of two coupled excitators (solid lines) following two input signals with a short interstimulus interval (ISI) of 80 ms are shown in Figure 10. Here the first stimulus is delivered to the first excitator unit and the second stimulus to the second excitator unit. A comparison with the uncoupled trajectories is made (dotted lines). It can be clearly seen that the first system is delayed because of the coupling so that a more simultaneous coordination dynamics—

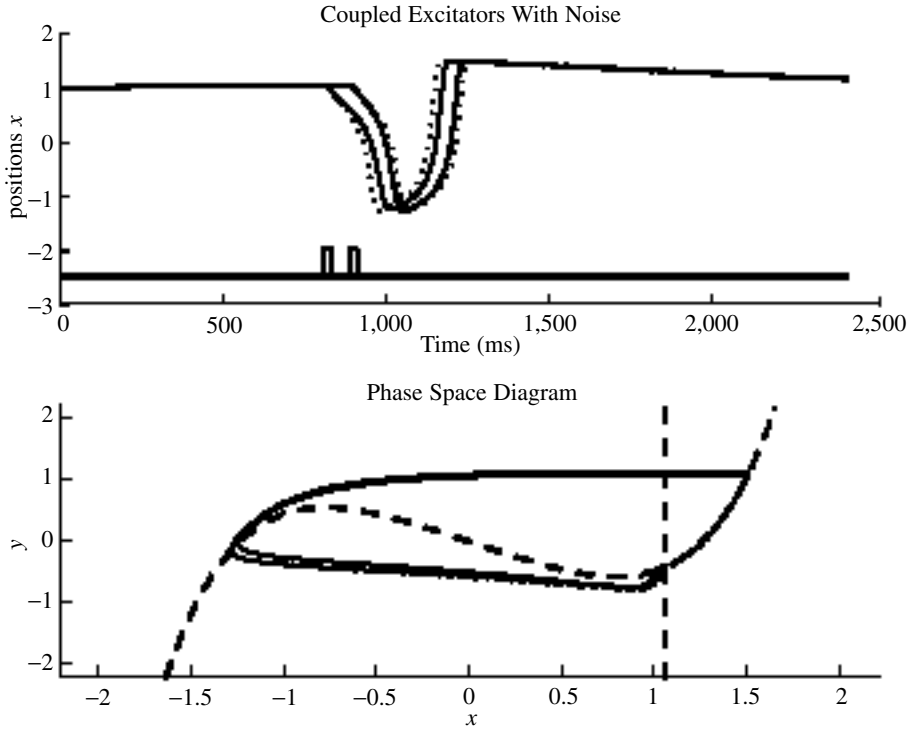

FIGURE 10. Convergence. The time series of two coupled excitators (solid lines) and two uncoupled excitators (dotted lines) following two consecutive stimuli are shown in the top panel. The interstimulus interval is 80 ms. Each input signal excites only one of the excitator units. The effect of the coupling is a convergence of the trajectories. The phase space trajectories in x, y coordinates are plotted in the bottom panel. The dashed lines indicate the nullclines used in the simulation.

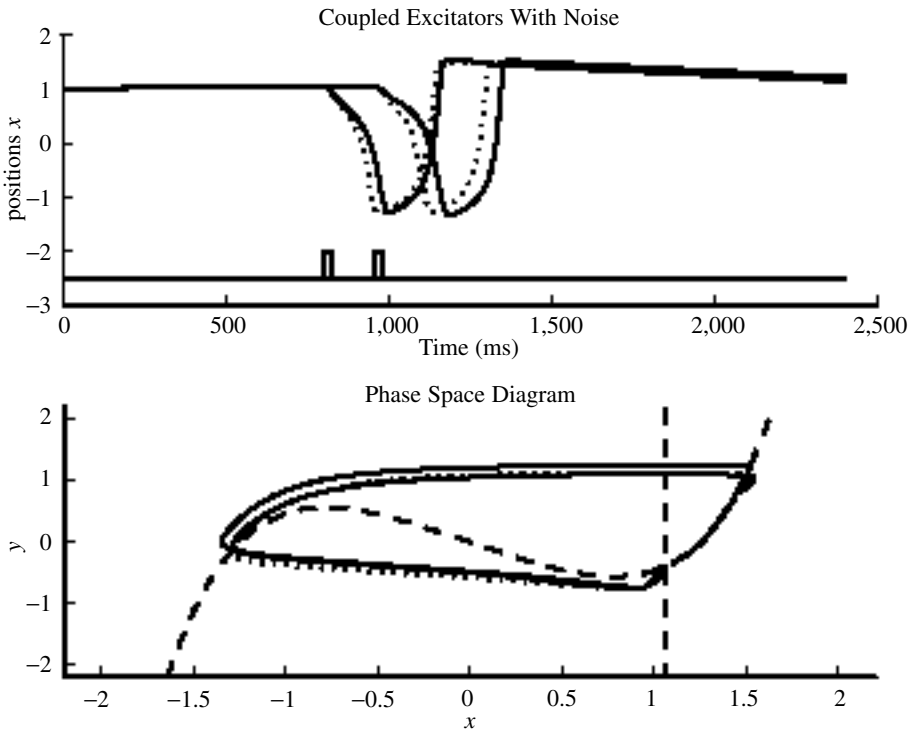

FIGURE 11. Divergence. The same situation as in Figure 10 is shown; only the interstimulus interval between the two inputs is increased to 160 ms. The time series in the top panel of the coupled excitators (solid lines) display a delay compared with that of the uncoupled excitators (dotted lines).

that is, convergence—can be achieved. Both couplings, the fully sigmoidal and its truncated form, the HKB coupling, accomplish that phenomenon.

The same situation as before is shown in Figure 11, only the ISI of the two consecutive stimuli has been increased to 160 ms. Again, the trajectories converge initially, such that the first excitator is delayed as in the previous case. But upon reaching a critical value of the trajectory distance, $d = |x_1 - x_2| \approx 2.6$ computational space units around time point 1,000 ms, the trajectories start diverging. As a consequence, both excitators are delayed with respect to the uncoupled system and also with respect to each other. Such acceleration phenomena have been observed experimentally (Kelso, Putnam, & Goodman, 1983; Kelso et al., 1979). The divergence cannot be observed when one uses a sigmoidal coupling, because the divergence condition in Equation 18 cannot be satisfied.

To illustrate the quantitative degree of convergence and divergence, we calculated the mean time delay between coupled and uncoupled excitator units. The mean time difference (upper graphs) and its variance (lower graphs) as a function of the ISI are displayed in Figure 12. As a measure, we chose the time difference between the positions of two excitators when they cross $x = 1$ after a flexion–extension cycle (just before they enter the return phase). The mean time difference was computed from 11 trials as a function of the ISI. With a dynamics as defined in Equation 27, the coupled excitator units show convergence times of coordinated action up to 50

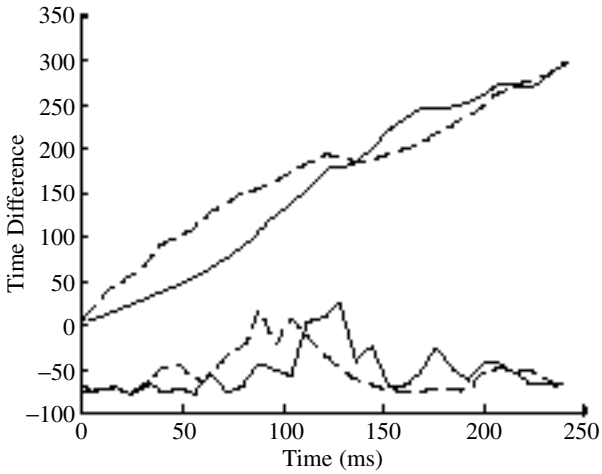

FIGURE 12. The mean time difference (upper graphs) and its variance (lower graphs) are plotted as a function of the interstimulus interval (ISI). The dashed lines refer to the uncoupled situation, the solid lines to the coupled situation. The variance is not plotted on the same scale as the time difference graphs. The maximum variance is about 800 ms^2 at an interstimulus interval of approximately 130 ms.

ms for ISIs from 0 to 130 ms. For ISIs greater than 130 ms, the coupled system displays divergence, although to a smaller extent (up to 30 ms). For ISIs between 100 and 150 ms, the variance of the time difference of the coupled system (solid line) is greatly enhanced. Because the variance of the uncoupled system (dashed line) is also enhanced in a similar range of ISIs, it is implied that an increased sensitivity of the intrinsic excitator dynamics rather than the coupling is the cause of the increased variance.

Conclusions

What have we accomplished by developing a "minimal model" that we have named here the *excitator*? First, the excitator summarizes the mathematical properties that a two-dimensional dynamic system based on ordinary differential equations must have so that it can produce a set of behaviors, the most striking ones being discrete and rhythmic movements and false starts. Among other models, the HKB model (Haken et al., 1985), Schöner's (1990) model and many neuronal models, such as the FitzHugh–Nagumo system (FitzHugh, 1961), the Hodgkin–Huxley equations (Hodgkin & Huxley, 1952), and the Hindmarsh–Rose oscillator (Hindmarsh & Rose, 1982), are specific realizations of the excitator for special parameter settings, in the sense that all of the previous models produce only a subset of behaviors. The virtue of the current description is its generality, which is based on the discussion of topological elements of the flow in phase space such as separatrices and stability of fixed points. The existence of those structural features is invariant under homeomorphisms (see the Hartmann–Grobmann theorem, e.g., Guckenheimer & Holmes, 1983; Perko, 1991), and arguments on the actual implementation of the dynamics of the system become superfluous (Peper & Beek, 1998). Admittedly, however, the specifics of implementation become relevant when addressing the dynamics and its underlying neuronal substrate because, here, the material realization will provide us with additional information on the shape of the mathematical terms present in the excitator. As an example, neuronal response functions are typically understood to be sigmoidal, and their slope and height vary with the degree of attention (Freeman, 1992). Such identification of the sigmoidal response function with the excitator couplings provides us with an entry point to attentional or, more generally, cognitive influences on the behavioral system and constrains the vast space of possible modeling. We propose a specific realization of the excitator, which is not unique but which allows for explicit quantitative predictions. For example, we predict the existence of an attractive manifold in the phase space (the return phase after the overshoot) along which the system evolves for a duration on the order of 400 ms. The manifold constrains the flow in the phase space to a limited region and hence constrains the movement dynamics. The motion along the manifold has refractory properties, such that perturbations or additional stimuli will excite the movement system less effectively until the final rest state is reached. Furthermore, we postulate the existence of a separatrix in phase space and predict that the probability of the occurrence of false starts increases with decreasing distance to the separatrix. More specifically, shifts of the location of the equilibrium point in phase space toward the separatrix are predicted to cause more false starts. The probability of the occurrence of a false start will be a function of three factors: (a) distance between the fixed point and the separatrix, (b) strength of the flow away from the separatrix, and (c) noise strength. All three components are experimentally accessible and allow the calculation of a mean escape time, which is directly related to the probability of the occurrence of a false start (see Fuchs & Jirsa, 2000, and Schöner, et al., 1986, for stochastic treatments of rhythmic movements). An experimental demonstration of the existence of a separatrix (the backbone of the excitator) involves showing a correlation between the probability of a false start and the three just-mentioned components. Finally, a general discussion of coupled excitators leads us to the prediction that the timing of coordinated multilimb movements primarily depends on the difference in the positions of the effectors, a phenomenon first noted in slightly different form (Schöner, 1990). Our analysis shows that for ISIs of less than 130 ms, two movements tend to be executed synchronously; conversely, for ISIs of more than 130 ms, two movements tend to be executed sequentially. Both effects are on the order of 30 to 50 ms.

ACKNOWLEDGMENTS

Defense Advanced Research Projects Agency Grant NBCH1020010, and National Institute of Mental Health Grants MH42900 and MH01386 supported this work. The help of Felix Almonte and Collins Assisi during movement data collection is much appreciated. We thank Ajay Pillai for help during the final editorial process and two anonymous reviewers who provided very helpful comments.

NOTES

1. Note that Olympic standards allow a minimum of 100-ms reaction time only. Anything faster than that is considered a false start, according to Olympic regulations.

2. Excitable systems are not to be confused with excited or self-excited systems. The former refer to systems with an external driver, the latter refer to systems with a self-excitation term, typically negative damping.

REFERENCES

Amari, S. (1977). Dynamics of pattern formation in lateral-inhibition type neural fields. *Biological Cybernetics, 27,* 77–87.

Balasubramaniam, R., & Feldman, A. G. (2004). Guiding movements without redundancy problems. In V. K. Jirsa & J. A. S. Kelso (Eds.), *Coordination dynamics: Issues and trends* (pp. 155–176). New York: Springer.

Beek, P. J., Peper, C. E., & Daffertshofer, A. (2002). Modeling rhythmic interlimb coordination: Beyond the Haken-Kelso-Bunz model. *Brain and Cognition, 48*(1), 149–165.

Campbell, S. R., & Wang, D. (1998). Relaxation oscillators with time delay coupling. *Physica D, 111*(1–4), 151–178.

Collet, C. (1999). Strategic aspects of reaction time in world-class sprinters. *Perceptual and Motor Skills, 88*(1), 65–75.

Croot, K., Hodges, J. R., Xuereb, J., & Patterson, K. (2000). Phonological and articulatory impairment in Alzheimer's disease: A case series. *Brain and Language, 75,* 277–309.

Daffertshofer, A., Peper, C. E., & Beek, P. J. (2004). *Stabilization of bimanual coordination due to active inhibition—Evidence from phase transitions*. (Manuscript submitted for publication).

Feldman, A. G. (1980a). Superposition of motor programs. I. Rhythmic forearm movements in man. *Neuroscience, 5,* 81–90.

Feldman, A. G. (1980b). Superposition of motor programs. II. Rapid flexion of forearm in man. *Neuroscience, 5,* 91–95.

FitzHugh, R. (1961). Impulses and physiological states in theoretical models of nerve membrane. *Biophysical Journal, 1,* 445–466.

Freeman, W. J. (1992). Tutorial on neurobiology: From single neurons to brain chaos. *International Journal of Bifurcation and Chaos, 2,* 451–482.

Fuchs, A., & Jirsa, V. K. (2000). The HKB model revisited: How varying the degree of symmetry controls dynamics. *Human Movement Science, 19*(4)*,* 425–449.

Fuchs, A., Jirsa, V. K., & Kelso, J. A. S. (2000). Theory of the relation between human brain activity (MEG) and hand movements. *Neuroimage, 11,* 359–369.

Fuchs, A., Kelso, J. A. S., & Haken, H. (1992). Phase transitions in the human brain: Spatial mode dynamics. *International Journal of Bifurcation and Chaos, 2,* 917–939.

Fuchs, A., Mayville, J. M., Cheyne, D., Weinberg, H., Deecke, L., & Kelso, J. A. S. (2000). Spatiotemporal analysis of neuromagnetic events underlying the emergence of coordinative instabilities. *Neuroimage, 12,* 71–84.

Gonzalez, D. L., & Piro, O. (1987). Global bifurcations and phase portrait of an analytically solvable nonlinear oscillator: Relaxation oscillations and saddle-node collisions. *Physical Review A, 36,* 4402–4410.

Grossberg, S., Pribe, C., & Cohen, M. A. (1997). Neural control of interlimb oscillations. I. Human bimanual coordination. *Biological Cybernetics, 77,* 131–140.

Guckenheimer, J., & Holmes, P. (1983). *Nonlinear oscillations, dynamical systems, and bifurcations of vector fields*. New York: Springer.

Hackley, S. A., & Valle-Inclán (1998). Automatic alerting does not speed late motoric processes in a reaction-time task. *Nature, 391,* 786–788.

Haken, H. (1983). *Synergetics. An Introduction* (3rd ed.). New York: Springer.

Haken, H. (1996). *Principles of brain functioning*. New York: Springer.

Haken, H. (2002). *Brain dynamics.* New York: Springer.

Haken, H., Kelso, J. A. S., & Bunz, H. (1985). A theoretical model of phase transitions in human hand movements. *Biological Cybernetics, 51,* 347–356.

Hindmarsh, J. L., & Rose, R. M. (1982). A model of the nerve impulse using two first-order differential equations. *Nature, 296*(5853), 162–164.

Hodgkin, A. L., & Huxley, A. F. (1952). A quantitative description of membrane current and its application to conduction and excitation in nerve. *Journal of Physiology, 117,* 500–544.

Jirsa, V. K. (2004). Information processing in brain and behavior displayed in large-scale topographies such as EEG and MEG. *International Journal of Bifurcation and Chaos, 14*(2), 679–692.

Jirsa, V. K., Friedrich, R., & Haken, H. (1995). Reconstruction of the spatiotemporal dynamics of a human magnetoencephalogram. *Physica D, 89,* 100–122.

Jirsa, V. K., Friedrich, R., Haken, H., & Kelso, J. A. S. (1994). A theoretical model of phase transitions in the human brain. *Biological Cybernetics, 71,* 27–35.

Jirsa, V. K., Fuchs, A., & Kelso, J. A. S. (1998). Connecting cortical and behavioral dynamics: Bimanual coordination. *Neural Computation, 10,* 2019–2045.

Jirsa, V. K., & Haken, H. (1996). Field theory of electromagnetic brain activity. *Physical Review Letters, 77,* 960–963.

Jirsa, V. K., & Haken, H. (1997). A derivation of a macroscopic field theory of the brain from the quasi-microscopic neural dynamics. *Physica D, 99,* 503–526.

Jirsa, V. K., & Kelso, J. A. S. (2000). Spatiotemporal pattern formation in neural systems with heterogeneous connection topologies. *Physical Review E, 62,* 8462–8465.

Jirsa, V. K., & Kelso, J. A. S. (2004). *Coordination dynamics: Issues and trends.* New York: Springer.

Kay, P. A., Kelso, J. A. S., Saltzmann, E. L., & Schöner, G. (1987). Space-time behavior of single and bimanual rhythmical movements: Data and limit cycle model. *Journal of Experimental Psychology, 13,* 178–192.

Kelso, J. A. S. (1977). Motor control mechanisms underlying human movement reproduction. *Journal of Experimental Psychology: Human Perception and Performance, 3,* 529–543.

Kelso, J. A. S. (1981). On the oscillatory basis of movement. *Bulletin of the Psychonomic Society, 18,* 63.

Kelso, J. A. S. (1995). *Dynamic patterns. The self-organization of brain and behavior.* Cambridge, MA: MIT Press.

Kelso, J. A. S. (2002). The complementary nature of coordination dynamics: Self-organization and the origins of agency. *Journal of Nonlinear Phenomena in Complex Systems, 5,* 364–371.

Kelso, J. A. S., Bressler, S. L., Buchanan, S., DeGuzman, G. C., Ding, M., Fuchs, A., et al. (1992). A phase transition in human brain and behavior. *Physics Letters A, 169,* 134–144.

Kelso, J. A. S., DelColle, J. D., & Schöner, G. (1990). Action-perception as a pattern formation process. In M. Jeannerod (Ed.), *Attention and performance XIII* (pp. 136–169). Hillsdale, NJ: Erlbaum.

Kelso, J. A. S., Fuchs, A., Lancaster, R., Holroyd, T., Cheyne, D., & Weinberg, H. (1998). Dynamic cortical activity in the human brain reveals motor equivalence. *Nature, 23,* 814–818.

Kelso, J. A. S., & Holt, K. G. (1980). Exploring a vibratory systems-analysis of human movement production. *Journal of Neurophysiology, 43*(5), 1183–1196.

Kelso, J. A. S., Putnam, C. A., & Goodman, D. (1983). On the space-time structure of human interlimb coordination. *Quarterly Journal of Experimental Psychology, 35A,* 347–375.

Kelso, J. A. S., Southard, D., & Goodman, D. (1979). On the coordination of two-handed movements. *Journal of Experimental Psychology: Human Perception and Performance, 5,* 229–238.

Kuramoto, Y. (1984). *Chemical oscillations, waves, and turbulence*. New York: Springer.

Mayville, J. M., Jantzen, K. J., Fuchs, A., Steinberg, F. L., & Kelso, J. A. S. (2002). Cortical and subcortical networks underlying syncopated and synchronized coordination revealed using fMRI. *Human Brain Mapping, 17,* 214–229.

Meyer-Lindenberg, A., Ziemann, U., Hajak, G., Cohen, L., & Berman, K. F. (2002). Transitions between dynamical states of differing stability in the human brain. *Proceedings of the National Academy of Sciences, 99*(17)*,* 10948–10953.

Murray, J. D. (1993). *Mathematical biology*. New York: Springer.

Nagashino, H., & Kelso, J. A. S. (1992). Phase transitions in oscillatory neural networks. *Science of Artificial Neural Networks, International Society for Optical Engineering, 1710,* 278–297.

Nunez, P. L. (1974). The brain wave equation: A model for the EEG. *Mathematical Biosciences, 21,* 279–297.

Nunez, P. L. (1995). *Neocortical dynamics and human EEG rhythms.* Oxford, England: Oxford University Press.

Peper, C. L. E., & Beek, P. J. (1998). Are frequency-induced transitions in rhythmic coordination mediated by a drop in amplitude? *Biological Cybernetics, 79*(4), 291–300.

Perko, L. (1991). *Differential equations and dynamical systems*. New York: Springer.

Polit, A., & Bizzi, E. (1978). Processes controlling arm movements in monkeys. *Science, 201,* 1235–1237.

Polit, A., & Bizzi, E. (1979). Characteristics of motor programs

underlying arm movements in monkeys. *Journal of Neurophysiology, 42,* 183–194.
Postma, A. (2000). Detection of errors during speech production: A review of speech monitoring models. *Cognition, 77,* 97–131.
Pribe, C., Grossberg, S., & Cohen, M. A. (1997). Neural control of interlimb oscillations. II. Biped and quadruped gaits and bifurcations. *Biological Cybernetics, 77,* 141–152.
Robinson, P. A., Rennie, C. A., & Wright, J. J. (1997). Propagation and stability of waves of electrical activity in the cerebral cortex. *Physical Review E, 56,* 826.
Schmidt, R. A., & Gordon, G. B. (1977). Errors in motor responding, "rapid" corrections, and false anticipations. *Journal of Motor Behavior, 9,* 101–111.
Schmidt, R. A., & McGown, C. (1980). Terminal accuracy of unexpectedly loaded rapid movements. Evidence for a mass-spring mechanism in programming. *Journal of Motor Behavior, 12,* 149–161.
Schöner, G. (1990). A dynamic theory of coordination of discrete movement. *Biological Cybernetics, 63,* 257–270.
Schöner, G., Haken, H., & Kelso, J. A. S. (1986). A stochastic theory of phase transitions in human hand movement. *Biological Cybernetics, 53,* 247–257.
Sternad, D., Dean, W. J., & Schaal, S. (2000). Interaction of rhythmic and discrete pattern generators in single-joint movements. *Human Movement Science, 19*(4)*,* 627–664.
Strogatz, S. H. (1994). *Nonlinear dynamics and chaos.* Reading, MA: Addison-Wesley.
Wilson, H. R., & Cowan, J. D. (1972). Excitatory and inhibitory interactions in localized populations of model neurons. *Biophysical Journal, 12,* 1–24.
Wilson, H. R., & Cowan, J. D. (1973). A mathematical theory of the functional dynamics of cortical and thalamic nervous tissue. *Kybernetik, 13,* 55–80.
Wing, A. M., & Kristofferson, A. B. (1973). Response delays and the timing of discrete motor responses. *Perception and Psychophysics, 14,* 5–12.
Wright, J. J., & Liley, D. T. J. (1996). Dynamics of the brain at global and microscopic scales: Neural networks and the EEG. *Behavioral Brain Sciences, 19,* 285.

APPENDIX

Here we shall derive the constraints given in Equation 4 for the system defined in Equation 3.

A.1 Existence of Separatrix

The horizontal flow shall be given by $\dot{x} = x + y - g_1(x)$. In a neighborhood U of the origin $(x, y) = (0, 0)$, the smooth function $g_1(x)$ shall have the following Taylor expansion:

$$g_1(x) = \frac{1}{2!}\partial_x^2 g_1(0)x^2 + \frac{1}{3!}\partial_x^3 g_1(0)x^3 + \ldots \tag{28}$$

which means that $g_1(0) = 0$ and $\partial_x g_1(0) = 0$. Then, the horizontal flow in U is given by $y = -x$ sufficiently close to the origin and is repelling.

A.2 Existence of Fixed Point (x_0, y_0)

There will be n fixed points, if and only if the nullclines of Equation 3 intersect in n points in the phase space.

A.3 Stability of Fixed Point (x_0, y_0)

The stability of the fixed point is determined by the eigenvalues of the Jacobian L, defined as

$$L = \begin{pmatrix} (1-\partial_x g_1)\tau & \tau \\ -(1+\partial_x g_2)/\tau & -\partial_y g_2/\tau \end{pmatrix}, \tag{29}$$

where the partial derivatives are to be evaluated at (x_0, y_0). The eigenvalues are obtained from the characteristic polynomial $\det(L - \lambda I) = 0$, with I as the identity matrix, and read

$$\lambda = \frac{1}{2}[-\partial_y g_2/\tau - \tau(\partial_x g_1 - 1) \pm \sqrt{\text{root}}], \tag{30}$$

with

$$\text{root} = [\partial_y g_2/\tau + \tau(\partial_x g_1 - 1)]^2 - 4[\partial_y g_2(\partial_x g_1 - 1) + 1 + \partial_x g_2]. \tag{31}$$

To simplify that ugly term, we use the sequential time scale hierarchy present in relaxation oscillators, that is, $\tau \gg 1$, neglect $\partial_y g_2/\tau$, and write

$$\lambda = \frac{1}{2}\left\{\begin{matrix} -\tau(\partial_x g_1 - 1) \\ \pm\sqrt{\tau^2(\partial_x g_1 - 1)^2 - 4[\partial_y g_2(\partial_x g_1 - 1) + 1 + \partial_x g_2]} \end{matrix}\right\}. \tag{32}$$

If $\text{Re}|\lambda| < 0$, then the fixed point (x_0, y_0) is stable. That results in the stability conditions

$$\partial_x g_1 > 1 \text{ and } \partial_y g_2(\partial_x g_1 - 1) + 1 + \partial_x g_2 > 0. \tag{33}$$

A.4 Boundedness

The condition for sequential time scale hierarchy, $\tau \gg 1$, shall be satisfied. Then, the center manifold theorem applies (Perko, 1991) and the fast variable, x, may be adiabatically eliminated (Haken, 1983), $\dot{x} = 0$, such that all the horizontal flow is contracted to $y = -x + g_1(x) \approx g_1(x)$, sufficiently far away from the origin. We require that the inverse of g_1^{-1} exists at least locally in phase space, $x = g_1^{-1}(y)$. Then, the vertical phase flow may be expressed as

$$\dot{y} = -\frac{1}{\tau}\underbrace{\{g_1^{-1}(y) - a + g_2[g_1^{-1}(y), y]\}}_{G(y)}, \tag{34}$$

and will be directed toward the origin for large y, if and only if

$$G(y) = G(y \to \pm\infty) \to \pm\infty. \tag{35}$$

As a consequence, if the nonlinear function $g_1(x)$ satisfies $g_1(x \to \pm\infty) \to \pm\infty$ also, then it follows that the horizontal flow is always directed toward the origin for large x. A slightly stronger constraint for the boundedness of horizontal and vertical flow is obtained by requiring point symmetry: $g_1(-x) \xrightarrow{x \to \pm\infty} -g_1(x)$ and $G(-y) \xrightarrow{y \to \pm\infty} -G(y)$.

Submitted April 23, 2003
Revised December 4, 2003